COMPARISONS BETWEEN THE DIAGENESIS OF DIOCTAHEDRAL AND TRIOCTAHEDRAL SMECTITE, BRAZILIAN OFFSHORE BASINS

HUNG K. CHANG[1]

Department of Geological Sciences, Northwestern University
Evanston, Illinois 60201

FRED T. MACKENZIE AND JANE SCHOONMAKER

Department of Oceanography and Hawaii Institute of Geophysics
University of Hawaii, Honolulu, Hawaii 96822

Abstract—Burial diagenetic reactions of di- and trioctahedral clay minerals were compared in Brazilian offshore, basinal sediment sequences of Cretaceous age. Originally dioctahedral smectite-rich shales of three basins—Potiguar, Ceara, and Ilha de Santana—exhibited the classical smectite-to-illite burial pattern. Trioctahedral clay-rich shales and trioctahedral clay-mineral cements in sandstones, however, showed a burial sequence of saponite to mixed-layer chlorite/saponite with progressive increase in the percentage of chlorite layers with increasing burial depth.

The change from disordered to ordered interstratifications of chlorite/saponite occurred in the temperature range 60°–70°C at a vitrinite reflectance value of about 0.65. These values are lower than those found for the ordering of illite/smectite clays. Increasing substitution of Al for Si in tetrahedral sites, followed by fixation of interlayer hydroxide sheets was found to be the major chemical change promoting transformation of saponite to chlorite via corrensite.

Key Words—Brazil, Chlorite, Corrensite, Diagenesis, Illite, Interstratification, Saponite, Smectite, Trioctahedral, Vitrinite reflectance.

INTRODUCTION

An understanding of shale diagenesis requires knowledge of the reaction pathways of clay minerals as a function of burial depth. A survey of the literature shows that the best understood diagenetic reaction in pelitic sediments is still the one first proposed by Burst (1959) for dioctahedral clay-rich shales. The reaction pathway of smectite to mixed-layer illite/smectite (I/S) to illite with increasing burial depth has proven to be a reliable temperature indicator. More recently, McCubbin and Patton (1981) showed that the initial mineral composition and time also affect the I/S composition. The overall reaction may be a major sink for K^+, a major source of SiO_2, and possibly a minor source of other ions, such as Fe^{2+} and Mg^{2+} (Boles and Franks, 1979).

Little is known, however, about the reaction pathways involving mineralogical transformation of trioctahedral clay-rich shales during burial. Few studies have entailed investigations of mineralogical transformations accompanying burial of this sediment type, which is usually associated with volcanic and evaporitic rocks (Iijima and Utada, 1971, 1972).

The purpose of this paper is to present the chemistry and mineralogy of two compositionally distinct shale sequences, one rich in dioctahedral clay and the other rich in trioctahedral clay, and to discuss the mechanisms of clay mineral transformation during burial of these sediments. The major portion of the work deals with the reaction path of saponite to chlorite and leads to a new model of temperature-sensitive mineral alteration during shale diagenesis, particularly shales lacking I/S.

GEOLOGICAL FRAMEWORK

The present study involves Cretaceous shale sequences of non-marine and marine origin (Figure 1) located in the northern continental shelf of Brazil. Aptian age sediments and five late Cretaceous shales of the Cassipore, Ilha de Santana, Ceara, and Potiguar basins along the 2000-km coastline were studied (Figure 2). The northern Brazilian offshore basins formed after break-up and subsequent separation of Gondwanaland during the early Cretaceous. The last orogeny (Brasiliano cycle) that affected Gondwanaland began 1000 m.y. ago and ended in the early Cambrian (Almeida, 1976). During the Paleozoic Era, sediment accumulation took place in the Maranhão basin (Figure 2). These basement rocks—plutonic, metamorphic, and sedimentary—were the sources of sediment for the newly formed Cretaceous offshore basins (~130 m.y. ago).

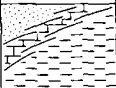[1] Present address: Petrobras-Cenpes, Ilha do Fundao, Rio de Janeiro, Brazil.

407

BRAZILIAN COASTAL BASINS MAJOR STRATIGRAPHIC DIVISIONS				
GEOLOGIC TIME	SEQUENCE	LITHOLOGY	ENVIRONMENT	TECTONIC EVOLUTION
TERTIARY LATE CRETACEOUS	MARINE		COASTAL AND OPEN MARINE	OPEN
SANTONIAN ALBIAN			MARINE SHALLOW PLATFORM	MARINE
APTIAN	EVAPORITIC		RESTRICTED MARINE AND LAGOONAL	GULF
NEOCOMIAN	CLASTIC NON-MARINE		DELTAIC LACUSTINE	RIFT - VALLEY
LATE JURASSIC			FLUVIAL	PRE-RIFT

Figure 1. Major stratigraphic divisions of the Brazilian coastal and offshore basinal sediments (Ponte *et al.,* 1980).

A striking compositional difference exists in the basement rocks, and three major geologic provinces can be distinguished (Figure 2). In the north, the Amazon craton (Suzsczynski, 1970) is characterized by metamorphosed volcano-sedimentary rocks of Lower Precambrian age; rocks from this area include mafic granulite, quartzite, amphibolite, mica schist, and granite (CPRM, 1979). In the east, the basement is dominated by plutonic and silicic metamorphic rocks such as granite, gneiss, and migmatite (Almeida *et al.,* 1976). Between these two old nuclei, the Maranhão basin is filled with Paleozoic sandstones and shales.

Because of these differences in source-area rock composition, the shales deposited in the Cretaceous offshore basins also vary in composition. Dioctahedral clay-rich shales have been found in the Potiguar, Ceara and Ilha de Santana basins, whereas trioctahedral clay-rich shales have been found in the Cassipore basin. Present-day geothermal gradients of the Cassipore, Ilha de Santana, Ceara, and Potiguar basins are, respectively, 22°, 28°, 31°, and 33°C/km. Based on a comparison of basin-subsidence curves and calculated paleo-isotherm curves, Chang (1983) demonstrated that the maximum temperatures reached by the Brazilian basinal sediments of this study were never significantly higher than the present values. Because these basins had a similar geologic and thermal history (Chang, 1983), clay-mineral reaction pathways can be compared in the two, compositionally different, shale sequences.

ANALYTICAL TECHNIQUES

Scanning electron microscopy

Sandstone samples were examined petrographically, and those that appeared to contain chlorite/smectite (C/S) cement were prepared for scanning electron microscopy (SEM). Fresh-fractured surfaces were mounted on SEM stubs with Duco cement and coated with gold. Energy dispersive X-ray analyses (EDX) were made to help in the identification of the minerals.

X-ray powder diffraction (XRD) analysis

Core samples were analyzed with an Rigaku-RU200 X-ray diffractometer using CuKα radiation. Because of the indurated nature of the shales, the samples were first coarsely crushed, then disaggregated while immersed in distilled water using an ultrasonicator. The <2-μm fraction was separated by standard centrifugation techniques, and oriented clay aggregates were prepared by the smear-mounting technique described by Gibbs (1965). Samples were analyzed from 2° to 30°2θ. Three analyses of each sample were made: (1) untreated air-dried mounts; (2) samples after vapor solvation in ethylene glycol for 24 hr; and (3) samples heated at 490°C for 1 hr. In addition, selected samples were subjected to KCl saturation and acid treatment using HCl.

The I/S identification was made by measuring the peak positions of $(002)_{10}/(003)_{17}$ for randomly interstratified illite/ethylene glycol-saturated smectite, and $(003)_{17}/(005)_{27}$ or $(001)_{10}/(003)_{27}$ for ordered illite/ethylene glycol-saturated smectite following the procedure described by Reynolds and Hower (1970). The C/S identification was based on the procedures described by Hower (1981a). To obtain the proportions of layer types present in the mixed-layer clays, peak positions of $(001)_{14}/(001)_{17}$ for random C/S, and $(002)_{31}/(001)_{17 \text{ or } 14}$ for ordered chlorite/ethylene glycol-saturated smectite were determined.

Chemical analysis

Oxide analyses of sediments were made by inductively-coupled plasma emission spectrometry (ICP) using a Jarrel Ash Plasma Atomcomp direct-reading spectrometer system. The precision of the method and the analytical error are well within 5% of the amount present.

Chemical microanalysis

Carbon-coated polished sections of sandstone cemented with C/S were analyzed with an energy dispersive X-ray fluorescence analyzer for Na, K, Ca, Mg, Fe, Mn, Al, Si, Cr, and Ti. An accelerating potential of 15 kV and beam current of 0.12 μA were used; each grain was probed for 60 s. Spectra were corrected for background, deadtime, drift, and matrix. The analytical error after these corrections is estimated to be less than 5%.

RESULTS

Dioctahedral clay diagenesis

Mineralogical changes with depth. Most workers agree that diagenesis of dioctahedral clay-rich shales in-
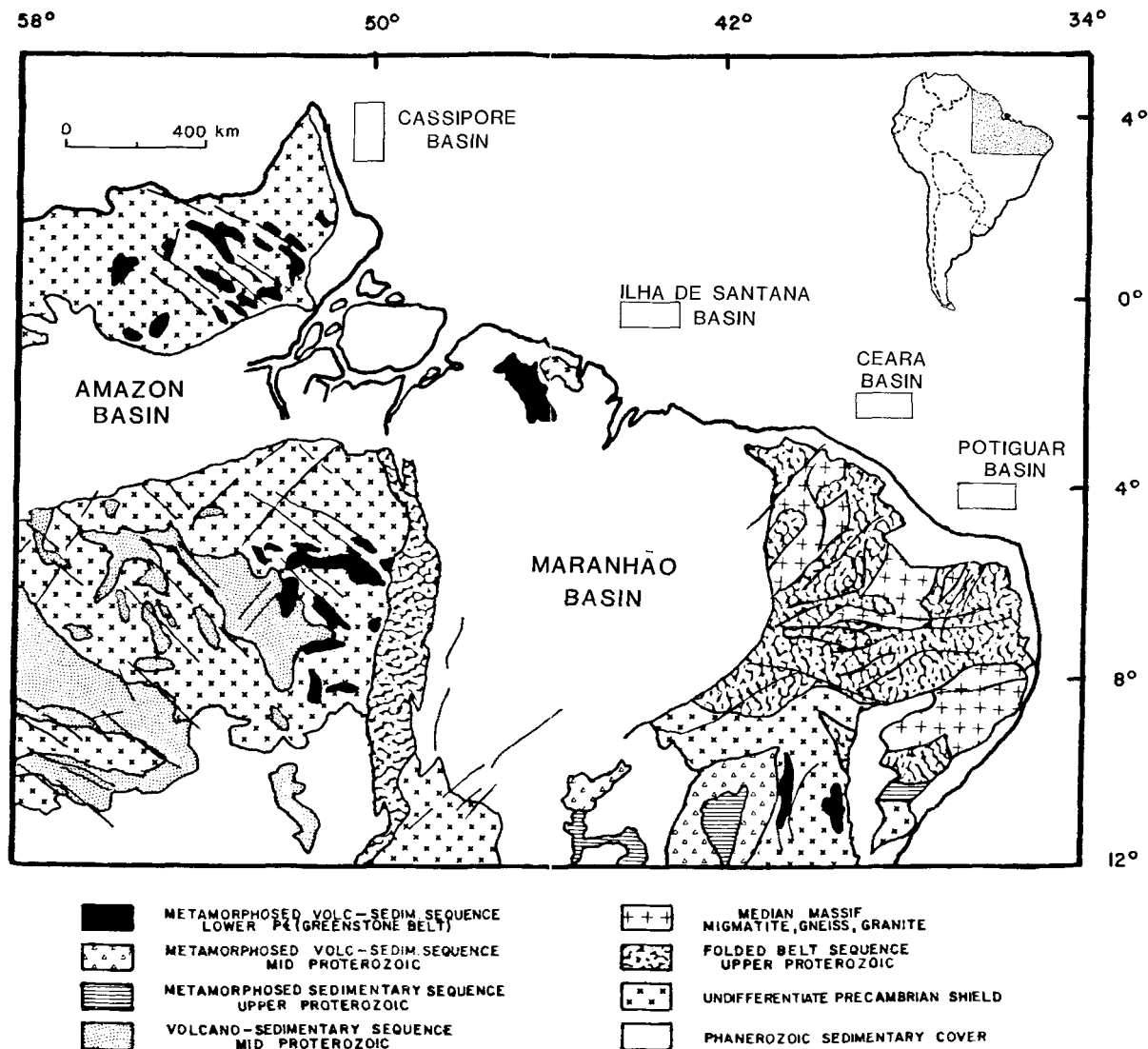
Figure 2. Tectonic map of northern Brazilian continent (CPRM, 1979). Offshore basins studied are delineated by the rectangles.

volves a smectite-to-illite transformation. In this work three basins, whose sediments derived primarily from weathering of granitic and gneissic terrains, exhibit the burial-induced sequence of smectite to illite. Thirty-four clay samples from cores in the depth range 1200–4700 m were analyzed from Ilha de Santana, Ceara, and Potiguar basins. Representative XRD profiles are shown in Figure 3.

The Ilha de Santana shales are characterized by a high content of chlorite and kaolinite, making the quantitative estimation of I/S composition difficult. A few samples contain exclusively chlorite. Shales of Ceara and Potiguar basins have high pyrite and carbonate contents. Potiguar basin shales show the greatest chemical contrast with respect to those of the other basins.

They are especially enriched in K_2O (3.5–5.6 wt. %), which reflects the abundance of K-feldspar in the coarse fraction (Chang, 1983). This K enrichment may have influenced the rate of illitization of smectite (Perry and Hower, 1970; Hower et al., 1976; Boles and Franks, 1979).

Smectite-to-illite transformation. In the three basins studied, the increasing illite content of the I/S with depth appears to be a consequence of burial of the sediments. Ordering of I/S in all three basins was first encountered when the percentage of illite layers reached 70–75. The depths of onset of ordering, however, ranged from about 3000 m for Ceara and Ilha de Santana basins to 2200 m for Potiguar basin (Figure 4). Ran-
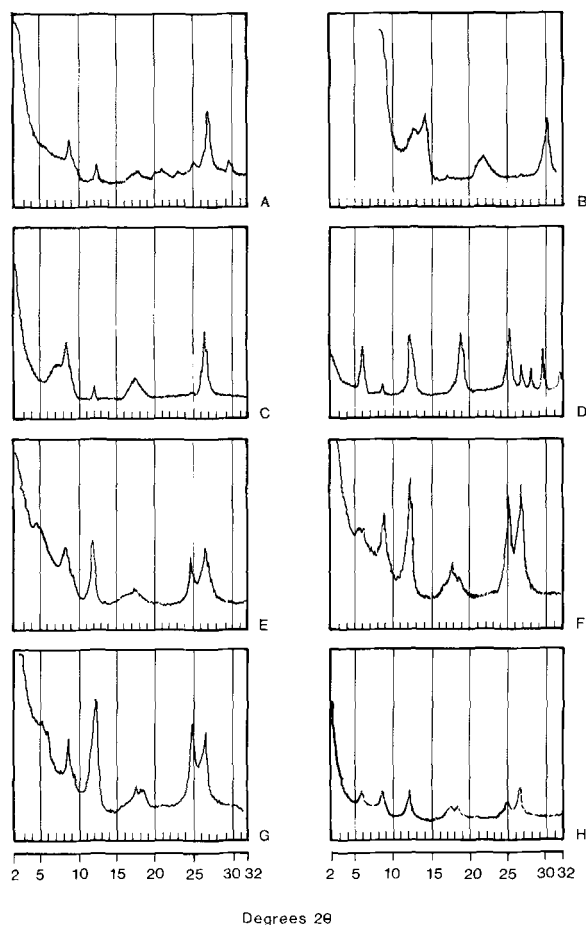
Figure 3. X-ray powder diffractograms of shales (<2-μm oriented aggregates) from the Ilha de Santana basin. CuKα radiation. Sample depths and major minerals are as follows: A. Depth = 2813.6 m; I_{70}/S_{30} (partial order), kaolinite, chlorite. B. Depth = 4700.0 m; I_{90}/S_{10} (R$\geq$3), chlorite? C. Depth = 3103.5 m; I_{78}/S_{22} (R=1), kaolinite. D. Depth = 3829.9 m; chlorite, illite. E. Depth = 1632.0 m; I_{50}/S_{50} (R=0), chlorite. F. Depth = 2972.5 m; I_{60}/S_{40} (partial order), kaolinite, chlorite. G. Depth = 2564.8 m; I_{60}/S_{40} (R=0), kaolinite, chlorite, illite. H. Depth = 3864.4 m; I_{80}/S_{20} (R=1), chlorite, kaolinite, illite.

Figure 4. Plot of illite content of illite/smectites (<2 μm) from dioctahedral clay-rich shales vs. depth. Solid symbols indicate ordered interstratification.

dom ordering (R=0) was found in the shallow samples, R=1 ordering in the deeper samples, and R=3 ordering in the deepest samples (Figure 3, terminology from Reynolds, 1980).

The Potiguar basin has a higher geothermal gradient than the other two basins which could have led to ordering of I/S at shallower depths in this basin than in Ceara or Ilha de Santana basins. Assuming a geothermal gradient of 33°C/km for Potiguar basin, however, the temperature of I/S ordering was about 90°C, whereas in the Ceara and Ilha de Santana basins, having average geothermal gradients of 31° and 28°C/km, respectively, the temperature of the ordering transition was about 110° and 100°C, respectively. Therefore,
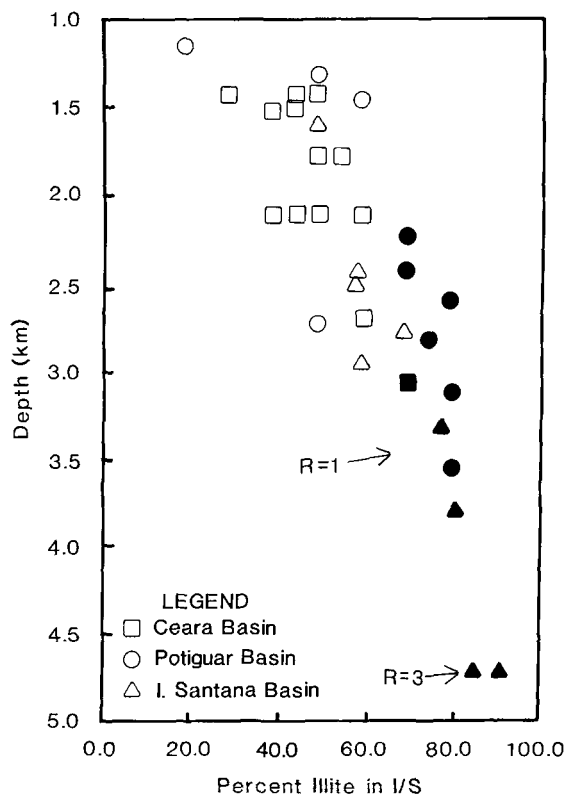
temperature alone does not appear to have been a sufficient constraint to explain the shallow depth of ordering of I/S in the Potiguar basin.

The transformation of smectite to illite requires that the net negative layer charge of the clay becomes sufficiently large to permit fixation of K and dehydration of interlayer space (Hower and Mowatt, 1966; Eberl, 1980). The substitution of Al for Si in the tetrahedral layer is the most probable mechanism leading to creation of negative layer charge (Foscolos and Kodama, 1974; Weaver, 1979). The reaction of smectite to illite, regardless of whether aluminum is conserved (Boles and Franks, 1979) or original smectite 2:1 layers are conserved (Hower *et al.*, 1976), requires a K supply. According to Heling (1974), the rate of illitization depends not only on the temperature, but also on the K concentration and mass transfer in the pore solution. He found that in porous and highly permeable sediments the illitization of smectite occurred at lower temperatures than in less porous and permeable units.

Potiguar basin shales contain more K-feldspar, as shown by semi-quantitative XRD analyses and as reflected in the high K_2O content of these sediments, than shales of the other two basins. Table 1 gives the bulk oxide composition of Brazilian basinal shales; Figure 5 shows the bulk composition of these shales on

Table 1. Whole-rock chemical analyses (wt. %) of Brazilian offshore basinal shales.

| Basin	Depth (m)	SiO_2	Al_2O_3	TiO_2	CaO	Na_2O	K_2O	Fe_2O_3	MgO	MnO	SrO
Ceara	1475.4	54.88	25.12	1.18	2.10	1.40	4.48	7.82	2.95	0.03	0.02
Ceara	2095.2	60.14	20.64	0.97	0.29	2.20	4.32	7.55	3.80	0.06	0.03
Potiguar	1212.5	68.90	10.71	1.04	0.86	1.60	3.45	10.07	3.23	0.10	0.02
Potiguar	2239.7	69.63	10.90	1.23	0.65	1.71	5.21	7.11	3.43	0.06	0.06
Potiguar	2420.4	67.41	9.94	1.02	2.19	2.09	4.67	9.18	3.40	0.06	0.03
Potiguar	3146.0	68.79	9.40	0.97	2.27	1.71	5.58	7.21	3.94	0.07	0.03
Potiguar	3568.0	67.79	13.06	1.07	0.95	1.53	4.66	7.71	3.16	0.05	0.02
I. Santana	1632.0	63.58	19.50	0.93	0.73	1.67	2.77	7.60	3.13	0.05	0.03
I. Santana	2562.4	63.25	17.71	0.91	1.07	1.94	2.70	8.89	2.97	0.52	0.03
I. Santana	2972.5	62.47	19.59	0.90	0.97	2.01	2.86	8.13	2.96	0.07	0.03
I. Santana	3302.6	62.12	18.52	0.90	0.71	1.84	3.23	8.84	3.74	0.08	0.02
I. Santana	3829.9	64.54	16.62	0.79	1.27	1.68	2.96	7.77	4.23	0.09	0.03
Cassipore	1511.0	61.34	16.65	1.01	2.36	2.41	2.17	9.40	4.50	0.11	0.03
Cassipore	1996.5	61.26	15.37	1.12	2.74	2.34	2.36	9.59	5.08	0.11	0.02
Cassipore	2541.5	60.77	15.21	1.03	4.75	2.35	1.95	0.81	3.90	0.17	0.04
Cassipore	2730.0	59.61	17.85	1.16	2.54	2.27	3.63	8.43	4.37	0.11	0.03
Cassipore	3065.0	69.52	14.01	0.97	1.17	1.43	2.55	7.41	2.83	0.08	0.02
Cassipore	3429.7	68.97	14.58	0.98	1.36	1.58	2.61	6.89	2.95	0.06	0.02

the triangular composition diagram, Na_2O-K_2O-Al_2O_3. Solution of K-feldspar during burial diagenesis could lead to substantial transfer of K from the feldspar into the pore solution of the shales. This transfer of K from feldspar to solution could produce a relatively high and sustained activity of K^+ in Potiguar shale pore waters, thereby promoting a shallower depth of ordering of I/S than in shales of the other two basins. Unfortunately, chemical analyses of pore waters from the shale units are not available.

Trioctahedral clay diagenesis

Corrensite and chlorite/saponite characteristics and occurrence. The term corrensite was proposed by Lippmann (1954) to describe a mixed-layer clay mineral with a regular alternation of chlorite and swelling chlorite. The term has subsequently been employed to describe a variety of regularly interstratified chlorite and expandable clays. The corrensite (defined in Bailey *et al.* (1982) as a 1:1 regular interstratification of trioctahedral chlorite and either trioctahedral smectite or trioctahedral vermiculite) from the Cassipore basin consists of a regular interstratification of chlorite and saponite. An ideal composition for corrensite is

$$R^+_{0.15}(Mg_4Al_{0.5})(Si_{3.35}Al_{0.65})O_{10}(OH)_5,$$
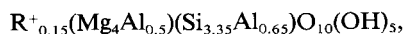
where Mg is commonly substituted for by Fe. In Brazilian sediments a typical composition as determined by EDX analysis of corrensite cement from a sandstone is

$$Ca_{0.06}Na_{0.01}(Fe_{2.30}Mg_{1.36}Ti_{0.02}Al_{0.084})-$$
$$(Si_{2.94}Al_{1.06})O_{10}(OH)_5.$$
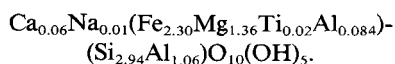
Chlorite/expandable clay mixed-layer minerals have been reported from a variety of environments and li-

thologies (Kubler, 1973). Corrensite has been found with evaporite rocks, in particular in Permo-Triassic evaporitic sequences (Lippmann, 1954, 1956; Martin-Vivaldi and MacEwan, 1957; Grim *et al.,* 1960; Fournier, 1961; Maurel, 1962; Kubler, 1963; Kopp and Fallis, 1974), and with carbonates (Eardley *et al.,* 1956; Bradley and Weaver, 1956; Peterson, 1961; Esquevin and Kulbicki, 1963). It commonly occurs in volcanogenic sequences and associated clastic sediments (Stephen and MacEwan, 1951; Kubler, 1973; Iijima and Utada, 1971; Wilson, 1971; Kubler *et al.,* 1974; Pevear and Whitney, 1982). Similar material has been reported in mafic intrusions (Sigvaldason and White, 1961; Harvey and Beck, 1962; Tomasson and Kristmannsdottir, 1972; Blatter *et al.,* 1973; Furbish, 1975). Experimentally (Iiyama and Roy, 1963; Wyart and Sabatier, 1966; Velde, 1977; Whitney, 1983) corrensite has been formed from smectites.
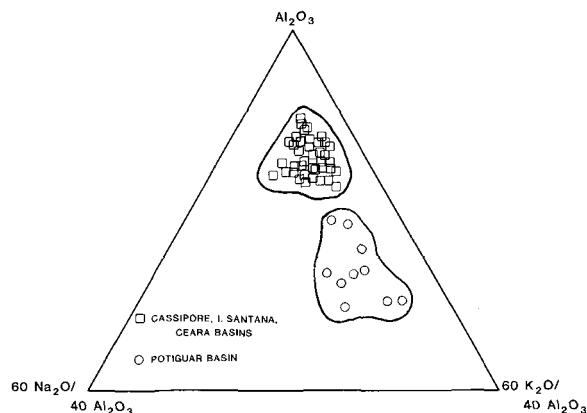

Figure 5. Na_2O-K_2O-Al_2O_3 ternary composition diagram of Brazilian basinal shales.
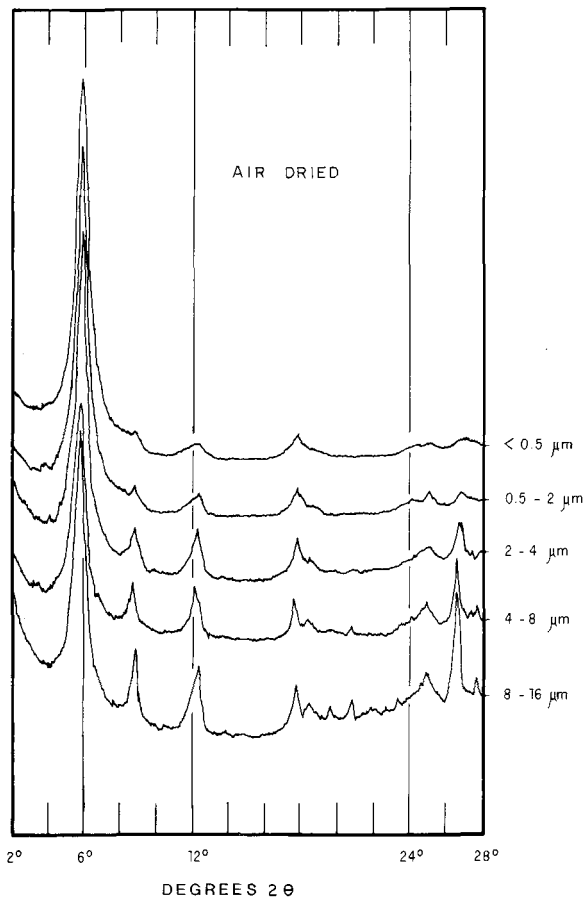
Figure 6.   X-ray powder diffractograms of oriented aggregates of various size-separated fractions of a typical shale sample from the Cassipore basin. CuKα radiation.

Figure 7.   X-ray powder diffractograms of <2-μm oriented aggregates of a typical saponite. Sample was immersed in KCl solution for 24 hr. A = air-dried; G = glycolated; H = heated to 490°C for 1 hr. CuKα radiation.

Saponite is a possible precursor of chlorite and C/S in tuffaceous and volcanic-rich sandstones (Iijima and Utada, 1971). It is also an important alteration product of deep-sea oceanic basalts (Melson and Thompson, 1973; Scarfe and Smith, 1977; Andrews, 1977; Seyfried *et al.,* 1978; Lawrence *et al.,* 1979). Seyfried and Bischoff (1979) produced saponite as a major product of basalt-seawater reactions in their hydrothermal experiments. Wilson *et al.* (1968) reported saponite and regularly interstratified chlorite/expandable clay from metamorphosed limestones in Scotland. Saponite was detected in fault zones of the Barbados accretionary prism (Schoonmaker, 1986). The most common occurrence of this trioctahedral smectite, however, is in mafic volcanic rocks. The iron-rich variety of saponite, the same as that encountered in sediments of Cassipore basin, was first observed in Tertiary "iron sand" beds associated with tuffs in Japan (Sudo, 1954; Sudo and Shimoda, 1978). This saponite composition also has been found in amygdales and fissures of basalt and andesite (Seyfried *et al.,* 1978). In pyroclastic rocks and associated sediments, it is commonly found cementing
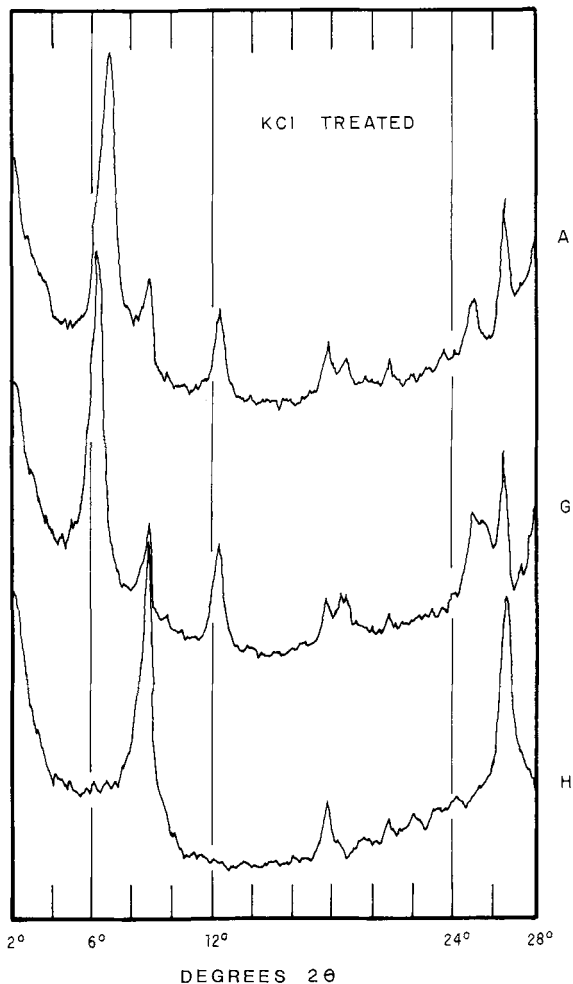
and replacing mineral grains and groundmass (Kohyama *et al.,* 1973).

Mineralogical changes with depth. The Cassipore basin provides a rare opportunity to study trioctahedral clay mineral diagenesis. Core samples of sandstones and shales from two wells were analyzed. The <2-μm size fraction was separated from 53 samples collected in the depth range 1300–3500 m. Figure 6 shows a series of diffractograms for various size fractions of a typical shale sample. In the coarser size fractions, the sample is significantly contaminated by detrital minerals, such as quartz and illite.

Trioctahedral smectite (saponite) and corrensite were found to be the dominant clay minerals in the <2-μm size fraction. Illite and I/S were present in minor amounts (<5%) in some samples. The illite is most likely of detrital origin. The saponite is actually an R=0
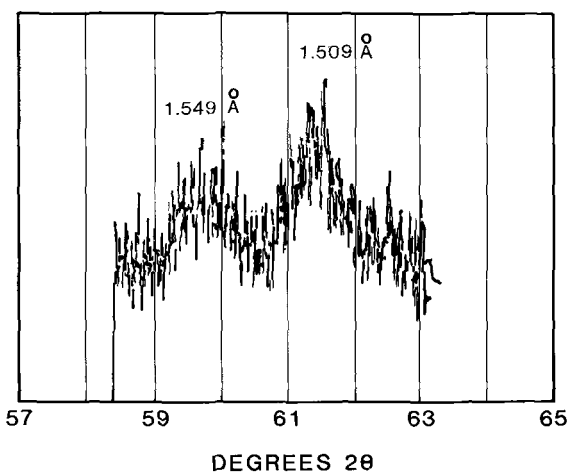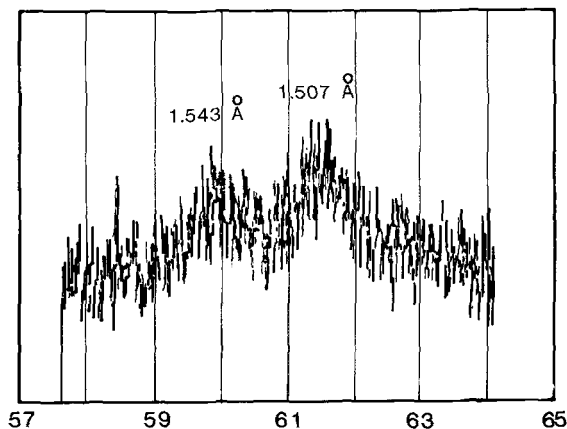
Figure 8.   X-ray powder diffractograms of 060 peaks of selected <2-μm oriented aggregates of shale samples from Cassipore basin. The 1.50-Å peak is indicative of illite, whereas the 1.54-Å peak is indicative of trioctahedral clays. CuKα radiation.

Figure 9.   X-ray powder diffractograms of <2-μm oriented aggregates of an untreated and HCl-treated saponite-rich sample. A = air dried; G = glycolated; H = heated to 490°C for 1 hr. CuKα radiation.

(random, mixed layer) C/S with about 20% chlorite layers. The saponite was recognized by its characteristic peak at 16.9 Å when glycolated and 12.8 Å when treated with KCl (Figure 7). The trioctahedral character of the clay was determined from the position of the 060 peak (Figure 8) and the chemical analysis, and corroborated by the destruction of the clay in HCl and the results of the heat treatment (Figures 7 and 9) (MacEwan and Wilson, 1980). The saponite is somewhat iron rich (Table 6). Corrensite was readily identified by its superlattice reflection at 31 Å and by reflections that shifted from 15.7 to 14.2 Å and from 7.8 to 7.1 Å with glycolation. The trioctahedral nature was deduced in a manner similar to that used for the saponite.

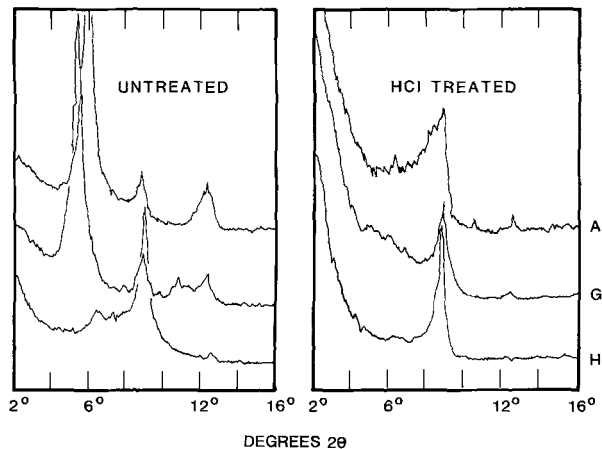As shown in Figures 10 and 11, R=0 C/S is important at shallow depths, whereas R=1 ordered C/S, eas-

ily recognized by its superlattice peak, is dominant at greater depths. To estimate the percentage of chlorite in the C/S, the calculated XRD patterns of trioctahedral C/S of Hower (1981a) were utilized. The precision of the estimations was limited by the presence in many patterns of broad peaks between 14.2 and 17 Å (6.18–5.2°2θ) and between 7.1 and 8.5 Å (12.42–10.40°2θ), indicating the presence of phases with a range of expandabilities. Broadening of the peaks (particularly the 7-Å peak) was more intense at greater depths. For these samples, the percentage of chlorite layers were estimated for the high- and low-angle extremes of the broad peaks. The average values obtained from these estimations are plotted in Figures 12 and 13.

Saponite-to-chlorite transformation. The best documented example of the diagenetic transformation of smectite to chlorite via C/S was noted in tuffaceous sediments of Japan (Iijima and Utada, 1971). The formation of corrensite at the expense of smectite was observed in a depth range equivalent to a temperature range of 85°–95°C. At higher temperatures smectite was not detected in the sediments. This temperature of first appearance of corrensite has been used as a paleotemperature indicator (Kubler, 1973; Hoffman and Hower, 1979).

The saponite-to-chlorite transformation is similar to that of montmorillonite to illite—change of an expandable phase into a nonexpandable one. The same geochemical variables applicable to dioctahedral clay diagenesis, such as temperature and bulk and fluid composition, affect the reaction rate of this transformation. The mechanisms of dewatering and hydroxide sheet fixation are similar to those of dewatering and potassium fixation in I/S and are examined below.

Using the ideal compositions of saponite and chlorite obtained for Cassipore basin clays (Chang, 1983), the
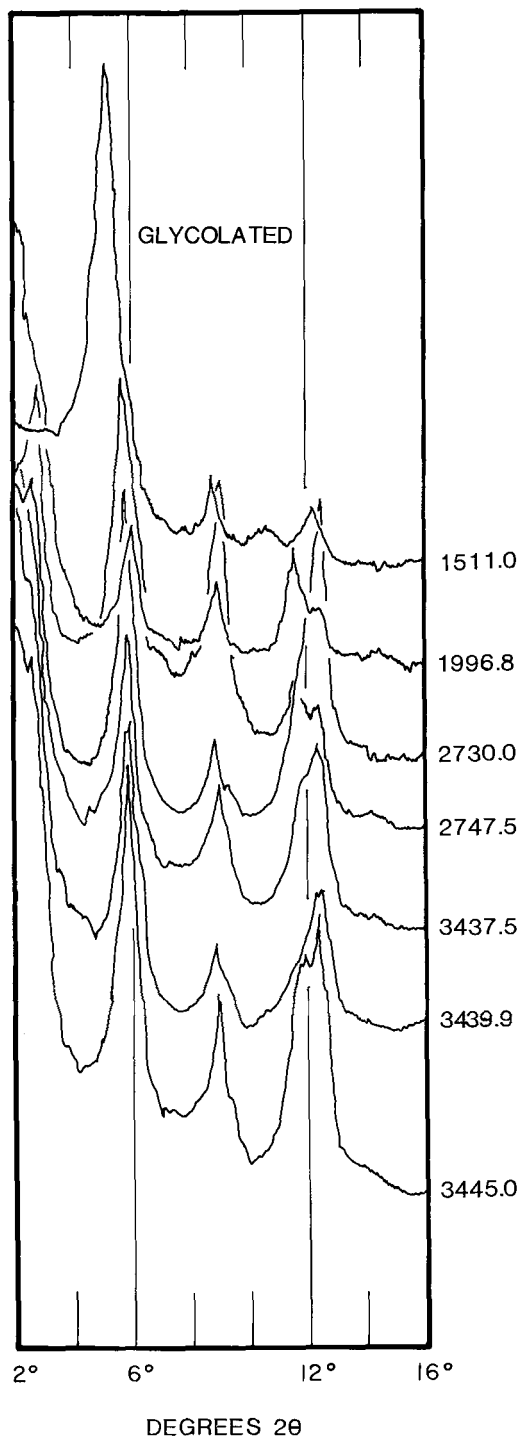
Figure 10.   X-ray powder diffraction profiles of <2-μm oriented aggregates of Cassipore basin shales from different depths of burial. CuKα radiation.
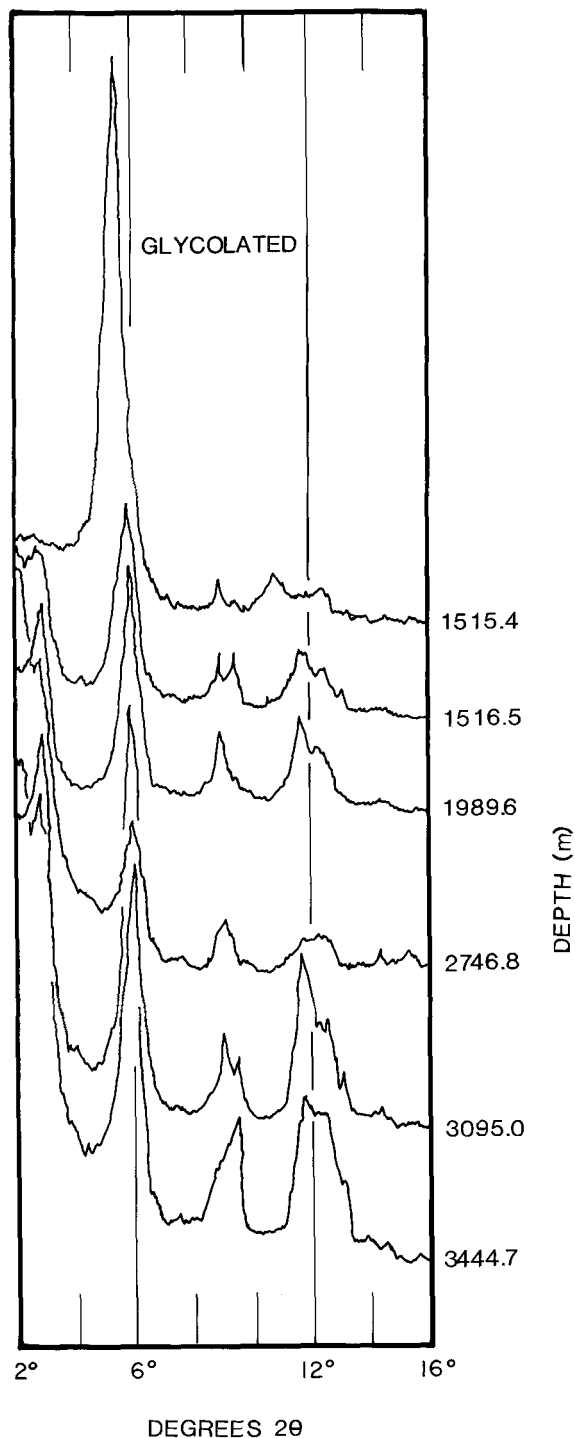
Figure 11.   X-ray powder diffraction profiles of <2-μm oriented aggregates of Cassipore basin sandstones at different depths of burial. CuKα radiation.

generalized chloritization reaction can be written in two ways: Reaction (1) follows the procedure of Hower *et al.* (1976), who assumed that the original smectite

(saponite) 2:1 layers remained intact, and that the mineralogical change involved only ionic substitution within that structure. Reaction (2) is written without
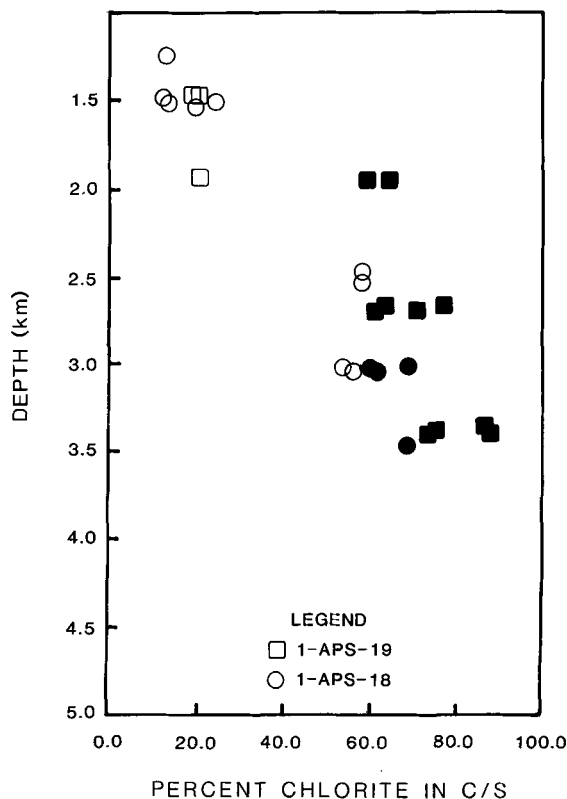
Figure 12.　Plot of average chlorite content of chlorite/saponites (<2 μm) from shales (Cassipore basin) vs. depth. Solid symbols indicate ordered interstratification.
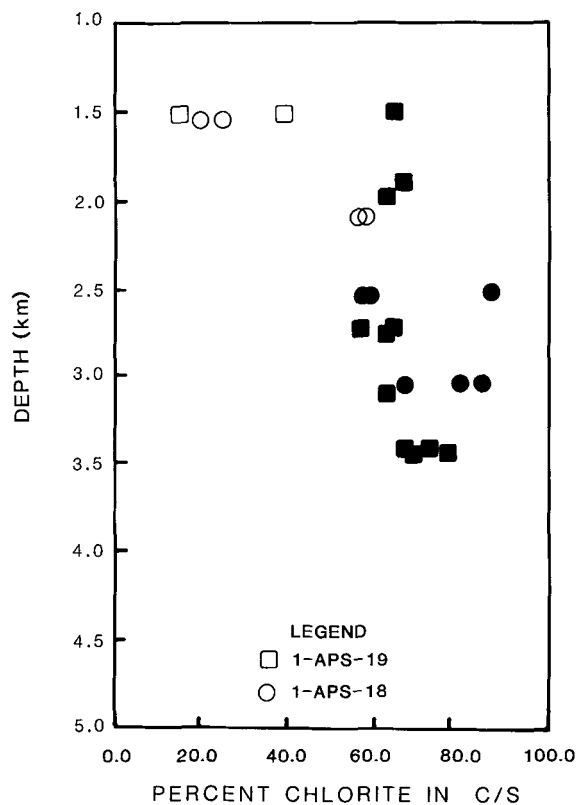
Figure 13.　Plot of average chlorite content of chlorite/saponite cement of sandstones (<2-μm size fraction) (Cassipore basin) vs. depth. Solid symbols indicate ordered interstratification.

conservation of the original 2:1 layers following Boles and Franks (1979). Al in reaction (1) behaves as a mobile component, whereas in reaction (2) Al is conserved.

$$Ca_{0.1}Na_{0.2}Fe_{1.1}MgAlSi_{3.6}O_{10}(OH)_2$$
saponite

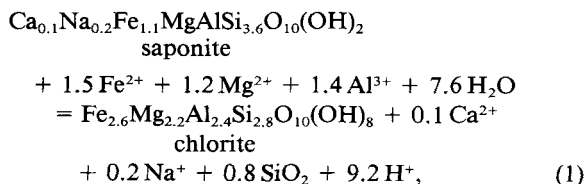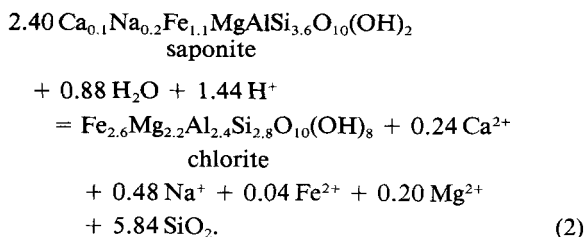$$+ 1.5\,Fe^{2+} + 1.2\,Mg^{2+} + 1.4\,Al^{3+} + 7.6\,H_2O$$
$$= Fe_{2.6}Mg_{2.2}Al_{2.4}Si_{2.8}O_{10}(OH)_8 + 0.1\,Ca^{2+}$$
chlorite
$$+ 0.2\,Na^+ + 0.8\,SiO_2 + 9.2\,H^+, \qquad (1)$$

and

$$2.40\,Ca_{0.1}Na_{0.2}Fe_{1.1}MgAlSi_{3.6}O_{10}(OH)_2$$
saponite

$$+ 0.88\,H_2O + 1.44\,H^+$$
$$= Fe_{2.6}Mg_{2.2}Al_{2.4}Si_{2.8}O_{10}(OH)_8 + 0.24\,Ca^{2+}$$
chlorite
$$+ 0.48\,Na^+ + 0.04\,Fe^{2+} + 0.20\,Mg^{2+}$$
$$+ 5.84\,SiO_2. \qquad (2)$$

The basic differences between the trioctahedral chloritization reaction and the dioctahedral illitization reaction are:

(1) The process of illitization requires K as well as H^+ or H_2O, whether the reaction procedes by conserving Al or the 2:1 smectite structure.
(2) Chlorite formation requires Fe, Mg, and H_2O to preserve the original smectite structure [reaction (1)], whereas for the Al conservation reaction [reaction (2)], only a supply of H_2O and H^+ is required.
(3) Interlayer space is occupied by K^+ for illitization, but chlorite forms by hydroxide sheet fixation.

One important consequence of hydroxide sheet fixation in trioctahedral smectite is that water is consumed in R^{2+}-hydroxide formation. Such a sink for water may affect the hydrodynamics of the basin and therefore be of importance to petroleum geologists who associate primary hydrocarbon migration with clay-mineral dewatering processes. The uptake of 7.6 moles of H_2O, as illustrated in reaction (1), is greater than the available interlayer water of smectite as calculated by Burst (1969). For two water layers of a total thickness of 5 Å per unit cell, he obtained eight molecules of water for a hexagonal water net and nine molecules of H_2O for an overpacked arrangement. In terms of the $O_{10}(OH)_2$ structural formula, these values corre-

Table 2.   Whole-rock chemical analyses (wt. %) of Brazilian offshore basinal sandstones.

Basin	Depth (m)	SiO₂	Al₂O₃	TiO₂	CaO	Na₂O	K₂O	Fe₂O₃	MgO	MnO	SrO
Potiguar	2269.0	79.75	10.12	0.07	2.23	2.23	3.38	0.93	1.22	0.02	0.02
Potiguar	2670.2	79.08	10.64	0.55	0.48	2.57	2.77	2.18	1.66	0.02	0.02
Potiguar	3125.7	83.17	9.03	0.21	0.63	0.99	3.88	1.22	0.83	0.02	0.01
Potiguar	3445.5	84.48	7.63	0.45	0.56	1.55	2.32	1.81	1.13	0.02	0.01
Potiguar	4417.0	80.99	9.52	0.40	1.92	2.99	1.49	1.98	2.64	0.03	0.03
I. Santana	1637.1	71.32	13.21	0.70	3.04	3.21	1.33	5.25	1.81	0.05	0.03
I. Santana	2569.0	72.35	13.73	0.44	1.55	3.65	1.24	5.26	1.67	0.07	0.03
I. Santana	2969.1	74.91	13.33	0.48	1.29	3.30	0.63	4.70	1.25	0.07	0.03
I. Santana	3298.0	80.35	10.14	0.26	1.42	3.58	0.41	2.55	1.20	0.06	0.02
I. Santana	3821.1	80.51	9.80	0.27	1.94	3.28	0.38	2.27	1.48	0.03	0.03
Cassipore	1516.0	73.14	12.19	0.67	2.92	2.50	1.66	4.68	2.13	0.06	0.03
Cassipore	1987.0	71.85	13.18	0.79	3.10	1.72	1.78	5.02	2.45	0.07	0.02
Cassipore	2547.0	68.31	14.79	0.80	3.52	2.88	1.92	4.63	3.03	0.08	0.02
Cassipore	2733.6	76.63	8.05	0.93	2.63	1.37	1.00	6.20	3.03	0.14	0.01
Cassipore	3061.0	78.13	7.29	0.83	4.20	1.23	0.88	5.12	2.24	0.07	0.01
Cassipore	3437.0	77.68	9.88	0.52	2.69	2.18	1.37	3.99	1.60	0.05	0.03

spond, respectively, to 4 and 4.5 moles of H_2O. Because for every mole of saponite only about 4 moles of H_2O are available in the interlayer, about 3.6 additional moles of H_2O are needed to complete the reaction. For example, if 20 cm^3 of saponite contained in 100 cm^3 of rock are transformed into chlorite [reaction (1)], assuming a density of 2.8 g/cm^3 and a molecular weight of 416 g/mole for saponite, an additional 8.72 cm^3 of H_2O is needed [(20 × 2.8/416) × 3.6 × 18]. If the transformation were to proceed by reaction (2), the amount of water needed (0.88 moles) is less than that required in reaction (1); this water easily can be obtained from the interlayer water of saponite, regardless of whether the water is present in hexagonal (4 moles) or overpacked (4.5 moles) arrangements.

C/S apparently orders at a shallower depth in sandstones than in shales. Figure 13 illustrates that corrensite in sandstones formed at 1500 m at about 60°C. In associated shales ordering started at about 2000 m and at about 70°C (Figure 12). The lower formation temperature of corrensite in sandstones does not seem to be related simply to bulk chemistry, because the bulk chemical compositions of both the sandstones and shales of the Cassipore basin are similar (cf. Tables 1 and 2). The pore water compositions, however, may be different in the sandstones and shales. The fluids in the sandstones are possibly exogenous, whereas those in the shales are more likely locally rock-dominated. Because pore water compositions are not available from Cassipore basin, this hypothesis cannot be tested. The higher permeability of sandstones may also be responsible for the ordering at shallower depths. Permeable and porous sandstone strata allow more local fluid/rock interaction and lead to more chemical exchange between the solid and fluid phases. Whether the reaction involves replacement of one phase by another or nucleation and growth of products, a higher water/rock ratio should accelerate both reactions because the

rate of mineral formation is primarily a function of the degree of supersaturation in solution.

Crystal chemistry. The compositional changes accompanying the smectite-to-illite transformation as deduced from published chemical analyses were summarized by Hower and Mowatt (1966) (see also Garrels and Mackenzie, 1974) and Hower (1981b). The main chemical changes with increasing percentages of illite layers are (1) a gain of interlayer K, (2) increased substitution of Al for Si in the tetrahedral layer, and (3) loss of octahedral Mg and Fe (Dunoyer de Segonzac, 1969, 1970). Weaver (1979) and Hower and Hall (1970) suggested that the change also involves the reduction of iron from Fe^{3+} to Fe^{2+} in octahedral sites of the clay mineral.

To investigate the compositional changes of the saponite-to-chlorite reaction, trioctahedral clays from the Cassipore basin sediments were chemically analyzed, and structural formulae were calculated. Structural formulae of C/S from the sandstones were calculated from EDX analyses (Table 3); those from the shales were calculated from ICP analysis of the <2-μm clay-size fraction. Because illite was present in the clay fraction of the shales, a correction for the presence of this phase was necessary. All K_2O was thus assumed to be in dioctahedral illite; this K_2O content and equivalent amounts of other oxides based on an ideal illite composition (Tardy and Garrels, 1974) were subtracted from the chemical analysis. The remaining oxides were normalized to 100% to obtain the composition of the saponite or corrensite phase. Tables 4 and 5 summarize the total cation content per structural formula of Cassipore basin clays and other trioctahedral clay mineral compositions obtained from published data. The cation distributions for samples from this work were derived according to the following rules: (1) Samples were considered to be either pure saponite $(O_{10}(OH)_2)$ or a

Table 3.   Chemical analyses (wt. %) of corrensites ($<2~\mu$m) in Cassipore basin sandstones.

Well	Depth (m)	SiO$_2$	Al$_2$O$_3$	TiO$_2$	CaO	Na$_2$O	K$_2$O	FeO	MgO	MnO	Cr$_2$O$_3$
APS-19	1516.3	37.04	20.36	0.46	2.09	0.52	0.13	30.56	6.69	1.86	0.23
APS-19	1996.0	39.92	16.89	0.81	1.35	1.38	0	23.47	15.17	0.90	0
APS-19	1996.0	37.48	15.55	0	3.17	0.70	0	26.52	15.52	0.62	0.31
APS-18	2552.5	35.83	16.16	0.12	1.91	2.93	0	29.76	12.82	0	0.44
APS-18	2552.5	36.61	15.85	0.08	1.16	1.07	0	30.14	14.62	0	0.37
APS-18	2552.5	44.30	17.39	0.06	1.01	3.54	0	22.22	10.96	0.13	0.29
APS-18	2552.5	37.59	16.37	0.01	1.92	1.58	0	28.65	13.34	0.09	0.28
APS-18	3066.3	33.79	21.49	0.38	0.48	1.05	0.52	32.22	9.92	0	0
APS-18	3066.3	32.53	21.86	0.13	0.29	0.32	0	33.54	10.42	0.42	0.43
APS-18	3066.3	33.77	21.24	0	0.30	0.06	0	33.71	9.67	0.78	0.37
APS-18	3066.3	35.34	19.46	0.38	0.65	0.06	0	33.02	11.00	0	0
APS-18	3066.3	35.07	20.52	0.29	0.61	0.87	0	30.12	12.23	0	0
APS-19	3438.0	33.41	18.25	0	2.63	0.08	0	32.94	12.04	0	0.21

1:1 C/S (O$_{10}$(OH)$_5$). (2) The tetrahedral layer was filled with Si and sufficient Al to occupy the four sites. (3) All Ca, Na, and K were assigned to interlayer exchangeable-cation positions. (4) All remaining cations were assigned to the octahedral part of the 2:1 layer and hydroxide sheets. (5) All Fe was assumed to be Fe^{2+}.

A few wet chemical analyses of Cassipore basin clays, particularly those from shales, show abnormally high total interlayer cation (Ca + Na + K) contents (Table 4). These high values were probably due to errors introduced by the illite correction. The analyses of saponites from shales (Table 4) also show low occupancy

of octahedral sites, more characteristic of a mixture of di- and trioctahedral clay minerals than of a pure saponite. Contaminant minerals other than illite may be present in the analyzed samples. Consequently, the cation distributions for the shales in Table 4 are somewhat suspect and have not been recalculated into structural formulae. Structural formulae for trioctahedral clay minerals from the sandstones and from published analyses are given in Tables 6 and 7.

The chemical data in Tables 4 and 5 provide important information on the systematic changes in the chemical composition of trioctahedral clay minerals during burial diagenesis. Chemical data for saponites

Table 4.   Cation content per unit formula of trioctahedral clay minerals of Cassipore basin.[1]

Well	Depth (m)	Tetrahedral		Octahedral			Interlayer
		Si	Al	(Mg + Fe^{2+} + Mn)	(Al + Cr)	Ti	(Ca + Na + K) (equiv.)
Sandstones							
Corrensite							
APS-19	1516.3	3.06	0.94	3.07	1.07	0.03	0.46
APS-19	1966.0	3.18	0.82	3.43	0.77	0.05	0.44
APS-19	1966.0	3.07	0.93	3.75	0.57	0	0.67
APS-18	2552.5	2.99	1.01	3.67	0.63	0.01	0.81
APS-18	2552.5	3.03	0.97	3.89	0.58	0.01	0.38
APS-18	2552.5	3.47	0.53	2.75	1.09	0.01	0.71
APS-18	2552.5	3.09	0.91	3.61	0.68	0	0.58
APS-18	3066.5	2.82	1.18	3.48	0.93	0.03	0.32
APS-18	3066.5	2.73	1.27	3.69	0.92	0.01	0.10
APS-18	3066.5	2.83	1.17	3.63	0.93	0	0.06
APS-18	3066.5	2.93	1.07	3.66	0.84	0.03	0.13
APS-18	3066.5	2.89	1.11	3.58	0.88	0.02	0.25
APS-19	3428.0	2.83	1.17	3.85	0.65	0	0.49
Shales							
Saponite							
APS-18	1239.0	3.74	0.26	1.28	0.89		1.02
APS-19	1511.0	3.95	0.05	1.89	0.54		1.09
APS-19	1517.0	3.95	0.05	1.89	0.54		0.59
APS-19	1989.2	3.83	0.17	2.96	0.21		1.13
Corrensite							
APS-19	1966.5	3.91	0.09	3.97	0.12		0.77
APS-19	2743.2	3.07	0.93	3.55	0.62		0.91

[1] Calculated from analyses in Table 3.

Table 5. Cation content per unit formula of trioctahedral clay minerals from the literature.

Tetrahedral		Octahedral		Interlayer (Ca + Na + K + Mg) (equiv.)	Source[1]
Si	$(Al + Fe^{3+})$	$(Mg + Fe^{2+})$	$(Al + Fe^{3+})$		
Saponite					
3.57	0.43	2.98	0.01	0.49	1
3.50	0.50	1.87	0.77	0.44	2
3.43	0.57	2.24	0.52	0.53	3
3.13	0.87	1.93	0.74	0.71	4
3.62	0.38	2.97	0.04	0.46	5
3.54	0.46	2.57	0.26	0.30	6
3.18	0.82	3.01	0.01	0.96	7
Corrensite					
3.12	0.87	2.18	1.75	0.23	8
Chlorite					
2.59	1.41	4.36	1.50		9
2.78	1.22	4.46	1.39		10
2.69	1.31	4.70	1.27		11
2.46	1.54	4.04	1.73		12
2.63	1.37	4.51	1.41		13
2.54	1.46	4.25	1.60		14

[1] 1 = Andrews (1977, p. 920); 2 = Melson and Thompson (1973, p. 712); 3 = Seyfried *et al.* (1978, p. 271); 4 to 7 = Sudo and Shimoda (1978, p. 238); 8 = April (1980, p. 5); 9 to 11 = Sudo and Shimoda (1978, p. 246); 12 to 14 = Sudo and Shimoda (1978, p. 249).

and corrensites from Cassipore basin shales are included in the following discussion; however, those data may not reflect the composition of pure phases (*vide supra*).

In Figure 14, the total exchangeable interlayer cation content of trioctahedral clays can be seen to decrease with increasing substitution of Al for Si in the tetrahedral layers. This trend reflects the transition from smectite, wherein net negative layer charge is balanced primarily by interlayer cations, to chlorite wherein the layer charge is balanced largely by hydroxide sheets. Along the line of slope = 1 in Figure 14, the tetrahedral charge created by Al-for-Si substitution is balanced by interlayer cations. Most saponite compositions from

the literature fall close to this line. The fact that the compositions of saponites of the present work fall well below the line also suggests that the material is not a pure phase. The compositons of the remainder of the samples fall above the line in the region where the octahedral layer and hydroxide sheet have a net positive charge sufficient to balance the negative charge of the tetrahedral layer. Although the points are somewhat scattered, a regular progression exists from saponite to corrensite to chlorite.

Total $Al + Fe^{3+}$ varies inversely with Si in trioctahedral clays (Figure 15). The total $Al + Fe^{3+}$ content of chlorite is high (as much as 3.5 atoms/unit formula), whereas that of saponite is low (<1.0 atom/unit formula). The C/S phases have compositions between those of chlorite and saponite. The compositions of deeply buried (>3000 m) C/S, however, approach that of chlorite, i.e., it is low in Si and exchangeable interlayer cations and high in total $Al + Fe^{3+}$. C/S from greater depths, as discussed above, contains 60–80% chlorite layers. The saponite samples plotted in Figure 15 roughly define a line along which one Al (or Fe^{3+}) is gained for every Si lost. This relationship presumably represents the initial tetrahedral substitution of Al and Fe^{3+} for Si during diagenesis. The corrensites and chlorites, however, fall on a line of steeper slope along which about 3 Al or Fe^{3+} ions are gained for every Si lost. This substantial increase in Al and Fe^{3+} reflects the addition of hydroxide sheets to the trioctahedral clay as well as substitution of these ions in the octahedral and tetrahedral layers.

Figure 16 illustrates the inverse relationship between Si and total $Mg + Fe^{2+}$. Chlorite has a high total $Mg + Fe^{2+}$ content (>4.0 atoms/unit formula) compared with the typical low values (<3.0 atoms/unit formula) for saponite. The general trend during the saponite-to-chlorite transformation is a gain of two $(Fe^{2+} + Mg)$ ions for each Si lost.

The above analyses indicate that the compositional changes in C/S that accompany increased numbers of chlorite layers involve a loss of interlayer cations (Fig-

Table 6. Structural formulae of trioctahedral clay mineral cements of Cassipore basin sandstones.

Well	Depth (m)	Structural formulae
APS-19	1516.3	$(Ca_{0.18}Na_{0.08}K_{0.01})(Fe_{2.11}Mg_{0.83}Ti_{0.03}Al_{1.05}Mn_{0.13}Cr_{0.02})(Si_{3.06}Al_{0.94})O_{10}(OH)_5$
APS-19	1996.0	$(Ca_{0.12}Na_{0.21})(Fe_{1.57}Mg_{1.80}Ti_{0.05}Al_{0.77}Mn_{0.06})(Si_{3.18}Al_{0.82})O_{10}(OH)_5$
APS-19	1996.0	$(Ca_{0.28}Na_{0.11})(Fe_{1.81}Mg_{1.89}Al_{0.57}Mn_{0.04}Cr_{0.02})(Si_{3.07}Al_{0.93})O_{10}(OH)_5$
APS-18	2552.5	$(Ca_{0.17}Na_{0.47})(Fe_{2.07}Mg_{1.59}Ti_{0.01}Al_{0.57}Cr_{0.03})(Si_{2.99}Al_{1.02})O_{10}(OH)_5$
APS-18	2552.5	$(Ca_{0.11}Na_{0.17})(Fe_{2.09}Mg_{1.81}Al_{0.58}Cr_{0.02}Ti_{0.01})(Si_{3.03}Al_{0.97})O_{10}(OH)_5$
APS-18	2552.5	$(Ca_{0.09}Na_{0.54})(Fe_{1.46}Mg_{1.28}Al_{1.08}Cr_{0.02}Mn_{0.01}Ti_{0.01})(Si_{3.47}Al_{0.53})O_{10}(OH)_5$
APS-18	2552.5	$(Ca_{0.17}Na_{0.25})(Fe_{1.97}Mg_{1.64}Al_{0.68}Cr_{0.02}Mn_{0.01})(Si_{3.09}Al_{0.91})O_{10}(OH)_5$
APS-18	3066.3	$(Ca_{0.05}Na_{0.17}K_{0.06})(Fe_{2.25}Mg_{1.23}Ti_{0.03}Al_{0.93})(Si_{2.82}Al_{1.18})O_{10}(OH)_5$
APS-18	3066.3	$(Ca_{0.03}Na_{0.05})(Fe_{2.36}Mg_{1.30}Ti_{0.01}Al_{0.89}Mn_{0.03}Cr_{0.03})(Si_{2.73}Al_{1.27})O_{10}(OH)_5$
APS-18	3066.3	$(Ca_{0.03}Na_{0.01})(Fe_{2.36}Mg_{1.21}Al_{0.93}Mn_{0.06}Cr_{0.02})(Si_{2.83}Al_{1.17})O_{10}(OH)_5$
APS-18	3066.3	$(Ca_{0.06}Na_{0.01})(Fe_{2.30}Mg_{1.36}Ti_{0.03}Al_{0.84})(Si_{2.93}Al_{1.07})O_{10}(OH)_5$
APS-18	3066.3	$(Ca_{0.05}Na_{0.14})(Fe_{2.08}Mg_{1.50}Ti_{0.02}Al_{0.88})(Si_{2.89}Al_{1.11})O_{10}(OH)_5$
APS-19	3438.0	$(Ca_{0.24}Na_{0.01})(Fe_{2.33}Mg_{1.52}Al_{0.65}Cr_{0.01})(Si_{2.83}Al_{1.17})O_{10}(OH)_5$

Table 7. Structural formulae of trioctahedral clay minerals from the literature.

Source[1]	Structural formulae	
1	$(Mg_{0.07}Ca_{0.12}Na_{0.08}K_{0.03})(Mg_{2.31}Fe^{2+}_{0.67}Al_{0.01})(Si_{3.57}Al_{0.43})O_{10}(OH)_2$	Saponite
2	$(Ca_{0.05}Na_{0.12}K_{0.22})(Mg_{1.16}Fe^{2+}_{0.71}Al_{0.77})(Si_{3.50}Ti_{0.02}Al_{0.48})O_{10}(OH)_2$	Saponite
3	$(Ca_{0.03}Na_{0.39}K_{0.08})(Mg_{1.94}Fe^{2+}_{0.30}Fe^{3+}_{0.52})(Si_{3.43}Al_{0.46}Fe^{3+}_{0.11})O_{10}(OH)_2$	Saponite
4	$(Ca_{0.27}Na_{0.07}K_{0.10})(Mg_{1.66}Fe^{2+}_{0.27}Fe^{3+}_{0.51}Al_{0.23})(Si_{3.13}Al_{0.87})O_{10}(OH)_2$	Saponite
5	$Ca_{0.23}(Mg_{1.52}Fe^{2+}_{1.45}Al_{0.04})(Si_{3.62}Al_{0.38})O_{10}(OH)_2$	Saponite
6	$Ca_{0.15}(Mg_{2.17}Fe^{2+}_{0.40}Fe^{3+}_{0.08}Al_{0.18})(Si_{3.54}Al_{0.46})O_{10}(OH)_2$	Saponite
7	$(Ca_{0.22}Na_{0.30}K_{0.22})(Mg_{1.02}Fe^{2+}_{1.99}Al_{0.01})(Si_{3.18}Al_{0.82})O_{10}(OH)_2$	Saponite
8	$(Ca_{0.07}Na_{0.09})(Mg_{1.54}Fe^{2+}_{0.64}Fe^{3+}_{1.31}Al_{0.44})(Si_{3.12}Al_{0.87})O_{10}(OH)_5$	Corrensite
9	$(Mg_{1.88}Fe^{2+}_{2.48}Fe^{3+}_{0.16}Al_{1.34})(Si_{2.59}Al_{1.41})O_{10}(OH)_8$	Chlorite
10	$(Mg_{2.88}Fe^{2+}_{1.58}Fe^{3+}_{0.25}Al_{1.14})(Si_{2.78}Al_{1.22})O_{10}(OH)_8$	Chlorite
11	$(Mg_{2.86}Fe^{2+}_{1.84}Fe^{3+}_{0.14}Al_{1.13})(Si_{2.69}Al_{1.31})O_{10}(OH)_8$	Chlorite
12	$(Mg_{0.17}Fe^{2+}_{3.87}Fe^{3+}_{0.45}Al_{1.28})(Si_{2.46}Al_{1.54})O_{10}(OH)_8$	Chlorite
13	$(Mg_{0.90}Fe^{2+}_{3.61}Fe^{3+}_{0.21}Al_{1.20})(Si_{2.63}Al_{1.37})O_{10}(OH)_8$	Chlorite
14	$(Mg_{1.01}Fe^{2+}_{3.24}Fe^{3+}_{0.40}Al_{1.20})(Si_{2.54}Al_{1.46})O_{10}(OH)_8$	Chlorite

[1] Refer to Table 5.

ure 14), increasing substitution of Al for Si in the tetrahedral layer (Figure 14), a gain in hydroxide sheet and octahedral layer Al + Fe^{3+} (Figure 15), and an overall increase in total Fe + Mg (Figure 16). These chemical changes are similar to those that attend the smectite-to-illite transformation. In both reactions, tetrahedral substitution of Al for Si results in an increase in charge deficiency. The basic difference between the two series of reactions involves the mechanisms by which the charge is balanced. Hydroxide sheets in chlorite are formed to compensate for the net negative charge in C/S, resulting in an overall increase in Al, Mg, and Fe. In I/S, charge is balanced by fixation of K in the interlayer positions during burial diagenesis.

Vitrinite reflectance

During catagenesis of solid organic matter the reflectance of vitrinite increases progressively with increasing temperature. Because no evidence of igneous or hydrothermal activity has been found in the Cre-
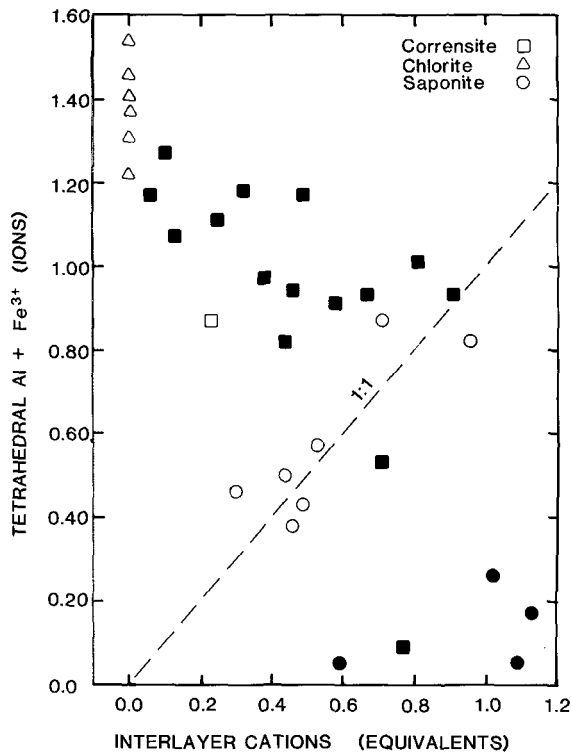

Figure 14. Plot of total interlayer cation (Na + K + Mg + Fe^{2+}) content vs. tetrahedral Al + Fe^{3+} per unit formula for trioctahedral clay minerals. Shaded symbols indicate analyses from this work.
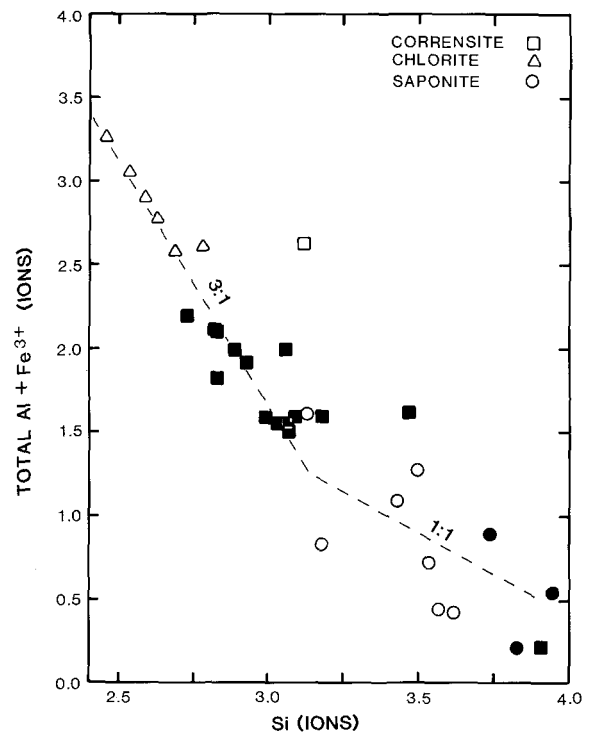

Figure 15. Plot of Si vs. total Al + Fe^{3+} per unit formula for trioctahedral clay minerals. Shaded symbols indicate analyses from this work.
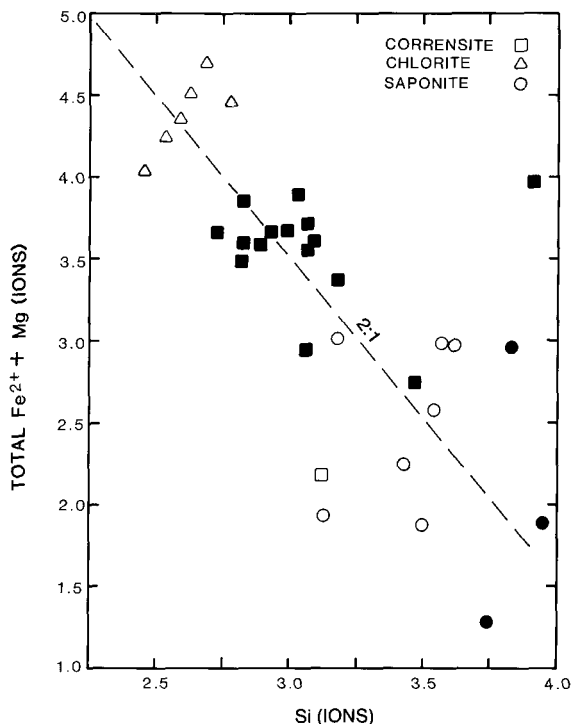
Figure 16. Plot of Si vs. total Fe^{2+} + Mg per unit formula for trioctahedral clay minerals. Shaded symbols indicate analyses from this work.

taceous sediments of the study area, the reflectance values are probably the result of temperature increase associated with burial.

Figure 17 is a plot of vitrinite reflectance (R_0) vs. present depth of burial. The data were obtained by S. G. Franks (Arco Oil and Gas Company) and L. P. Quadros (Petrobras, Brazil). R_0 values (Table 8) also suggest that the maximum temperatures reached by the sediments are compatible with their present depth of burial (Chang, 1983). The range of mean R_0 values is 0.59 to 0.98. Although the small number of samples has limited detailed correlation of R_0 values with temperature for all basins, the higher R_0 values of the Ilha de Santana basin samples compared with those from the Cassipore basin are in accord with the measured present-day thermal gradients in the area (Chang, 1983). The linear trend of R_0 with depth indicates that these sediments have not been subjected to significant changes in the geothermal gradient with depth which would have been expected to produce a break in the linear relationship between reflectance values and burial depth (Hunt, 1979).

CLAY MINERAL DIAGENESIS AS A PALEOTEMPERATURE INDICATOR

As discussed above, the transition from random to ordered (R=0 to R=1) interstratification in I/S and C/S is affected by bulk and pore water composition, per-

meability, and temperature. The importance of temperature in these diagenetic transformations is evidenced by the narrow range over which the ordering takes place, commonly within 30°C (90°–120°C) for I/S.

For Tertiary sediments of the Gulf Coast, Boles and Franks (1979), for example, found that the transition of random to ordered interlayering in I/S in Eocene shales occurs at 95°C. In Miocene-Pliocene rocks, Perry and Hower (1970) and Hower *et al.* (1976) reported temperatures between 90° and 110°C for the transition. More recently, Freed (1979) reported the temperature of transition to be about 120°C for shales of the Oligocene Frio Formation.

Unlike the smectite-to-illite transition, only a few studies have documented the temperature of the smectite-to-chlorite transformation. The temperature of 90°C, obtained by Iijima and Utada (1971) for the first appearance of corrensite in Neogene sediments of Japan, was used by Kubler (1973) and Hoffman and Hower (1979) as the temperature of corrensite formation.

Temperatures for the formation of ordered interstratification for I/S of Brazilian offshore basinal sediments are 90°, 100°, and 110°C for Potiguar, Ilha de Santana, and Ceara basins, respectively, and are similar to temperatures obtained for Gulf Coast sediments. The temperature of 70°C obtained for the first appearance of corrensite in Cassipore basin shales is 20°C lower than that reported by Iijima and Utada (1971). The vitrinite reflectance value of 0.65 at the depth of corrensite formation supports the argument that trioctahedral clay ordering starts at a lower temperature than I/S ordering. Ordering of I/S begins at a depth equivalent to vitrinite reflectance value of about 0.82.

CONCLUSIONS

On the basis of XRD and chemical data, several conclusions can be drawn concerning burial diagenesis of clay minerals in Brazilian shales and sandstones.

(1) I/S ordering took place between 90° and 110°C. The K_2O enrichment of Potiguar basin sediments may have contributed to the lower temperature of mixed-layer ordering in this basin.

(2) C/S ordering (corrensite) occurred at 70°C in shales and 60°C in sandstones. Permeability was probably responsible for the lower temperature of C/S ordering in the sandstones.

(3) Vitrinite reflectance values corroborate the lower temperature of corrensite formation with respect to that of R=1 ordered I/S. The reflectance values are 0.65 and 0.82 for ordered C/S and I/S formation, respectively.

(4) Published chemical analyses and those of Cassipore basin sediments indicate that the alteration process from saponite to chlorite involves a loss of interlayer cations, an increased substitution of Al and Si in
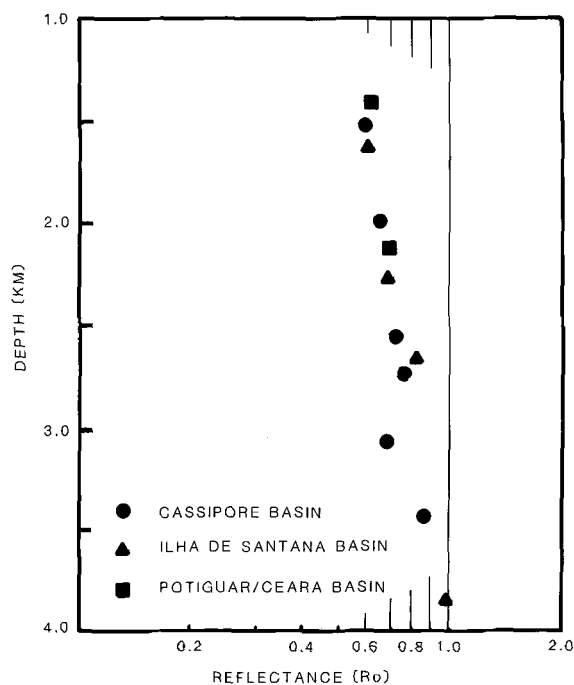
Figure 17.   Plot of vitrinite reflection values (R_0) vs. depth of burial. Reflectance values listed in Table 8.

Table 8.   Vitrinite reflectance values (R_0) measured in oil.

Well[1]	Depth (m)	Mean R_0	N^2	σ^3	BHT[4] (°C)
APS-18	1517.0	0.59	86	0.10	62
APS-18	1987.4	0.65	117	0.11	70
APS-18	2547.9	0.72	21	0.12	77
APS-19	2731.5	0.76	22	0.22	82
APS-18	3073.0	0.68	83	0.08	88
APS-19	3429.7	0.86	30	0.15	95
MAS-8	1631.0	0.60	88	0.12	62
MAS-11	2280.0	0.69	11	0.08	70
MAS-8	2676.5	0.82	112	0.14	93
MAS-8	3847.5	0.98	111	0.15	125
RNS-11	1403.0	0.62	85	0.11	67
CES-27	2119.0	0.69	25	0.07	82

[1] APS = Cassipore basin; MAS = Ilha de Santana basin; RNS = Potiguar basin; CES = Ceara basin.
[2] N = number of measurements.
[3] σ = standard deviation.
[4] BHT = corrected borehole temperature.

the tetrahedral layer, and a fixation of hydroxide sheets which compensate for the charge deficiency created by tetrahedral substitution. Hydroxide sheet formation results in increased contents of Mg, Fe, and Al.

ACKNOWLEDGMENTS

REFERENCES

Almeida, F. F. M. (1976) Origem e evolucao da Plataforma Brasileira: Div. Min. Geol. Dep. Nac. Prod. Min. Bol. 263, 65 pp.
Almeida, F. F. M., Hasui, Y., and Neves, B. B. B. (1976) The Upper Precambrian of South America: Bull. Inst. Geoscien. USP, 7, 45–80.
Andrews, A. J. (1977) Low-temperature fluid alteration of oceanic layer 2 basalts, DSDP leg 37: Canadian J. Earth Sci. 14, 911–926.
April, R. H. (1980) Regularly interstratified chlorite/vermiculite in contact metamorphosed red beds, Newark Group, Connecticut Valley: Clays & Clay Minerals 28, 1–11.
Bailey, S. W., Brindley, G. W., Kodama, H., and Martin, R. T. (1982) Report of the Clay Minerals Society Nomenclature Committee for 1980–1981: Clays & Clay Minerals 30, 76–78.
Blatter, C. L., Robertson, H. E., and Thompson, G. R. (1973) Regularly interstratified chlorite/dioctahedral smectite in dyke-intruded shales, Montana: Clays & Clay Minerals 21, 207–212.
Boles, J. R. and Franks, S. G. (1979) Clay diagenesis in Wilcox sandstones of southwest Texas: implications of smectite diagenesis on sandstone cementation: J. Sed. Petrology 49, 55–70.
Bradley, W. F. and Weaver, C. E. (1956) A regularly interstratified chlorite-vermiculite clay mineral: Amer. Mineral. 41, 497–504.
Burst, J. F., Jr. (1959) Postdiagenetic clay mineral environment relationship in the Gulf Coast Eocene: in Clays and Clay Minerals, Proc. 6th Natl. Conf., Berkeley, California, 1957, Ada Swineford, ed., Pergamon Press, New York, 327–341.
Burst, J. F., Jr. (1969) Diagenesis of Gulf Coast clayey sediments and its possible relation to petroleum migration: Amer. Assoc. Petrol. Geol. Bull. 53, 79–93.
Chang, H. K. (1983) Diagenesis and mass transfer in Cretaceous sandstone-shales sequences, offshore Brazil: Ph.D. dissertation, Northwestern Univ., Evanston, Illinois, 338 pp.
CPRM (1979) Projecto mapa Geologico do Brazil na escala 1:2.500.000: Companhia de Pesquisa de Recursos Minerais, Rio de Janeiro, Brazil.
Dunoyer de Segonzac, G. (1969) Les minéraux argileux dans la diagenèse passage au metamorphisme: Mem. Ser. Carte Geol. Als. Lorr. 29, 320 pp.
Dunoyer de Segonzac, G. (1970) The transformation of clay minerals during diagenesis and low-grade metamorphism: a review: Sedimentology 15, 281–346.
Eardley, J. W., Brindley, G. W., McVeagh, W. J., and Vanden

Heuvel, R. C. (1956) A regularly interstratified mont-morillonite-chlorite: *Amer. Mineral.* **41**, 258–267.

Eberl, D. D. (1980) Alkali cation selectivity and fixation by clay minerals: *Clays & Clay Minerals* **28**, 161–172.

Esquevin, J. and Kulbicki, G. (1963) Les minéraux argileux de l'Aptien Supérieur du Bassin d'Arzacq (Aquitaine): *Bull. Serv. Carte Geol. Als. Lorr.* **16**, 197–203.

Foscolos, A. E. and Kodama, H. (1974) Diagenesis of clay minerals from Lower Cretaceous shales of northeastern British Columbia: *Clays & Clay Minerals* **22**, 319–335.

Fournier, R. O. (1961) Regularly interlayered chlorite-vermiculite in evaporite of the Salado Formation, New Mexico: *U.S. Geol. Surv. Prof. Pap.* **424D**, 323–327.

Freed, R. L. (1979) Shale mineralogy of the No. 1 Pleasant Bayou geothermal test well: a progress report: in *Proc. 4th Geopressured-Geothermal Energy Conf., Univ. Texas, Austin, Texas, 1979, vol. 1*, 153–165.

Furbish, W. J. (1975) Corrensite of deuteric origin: *Amer. Mineral.* **60**, 928–930.

Garrels, R. M. and Mackenzie, F. T. (1974) Chemical history of the oceans deduced from post depositional changes in sedimentary rocks: in *Studies in Paleo-Oceanography*, W. W. Hay, ed., *Soc. Econ. Paleontol. Mineral. Spec. Publ.* **20**, 193–204.

Gibbs, R. J. (1965) Error due to segregation in quantitative clay mineral X-ray diffraction mounting techniques: *Amer. Mineral.* **50**, 741–751.

Grim, R. E., Droste, J. B., and Bradley, W. F. (1960) A mixed-layer clay mineral associated with an evaporite: in *Clays and Clay Mienrals, Proc. 8th Natl. Conf., Norman, Oklahoma, 1959*, Ada Swineford, ed., Pergamon Press, New York, 228–236.

Harvey, R. D. and Beck, C. W. (1962) Hydrothermal, regularly interstratified chlorite-vermiculite and tobermorite in alteration zones at Goldfield, Nevada: in *Clays and Clay Minerals, Proc. 9th Natl. Conf., 1960, Lafayette, Indiana*, Ada Swineford, ed., Pergamon Press, New York, 343–354.

Heling, D. (1974) Diagenetic alteration of smectite in argillaceous sediments of Rhinegraben (SW Germany): *Sedimentology* **21**, 463–472.

Hoffman, J. and Hower, J. (1979) Clay mineral assemblages as low grade metamorphic geothermometers: application to the thrust faulted disturbed belt of Montana, USA: *Soc. Econ. Paleontol. Mineral. Spec. Publ.* **26**, 55–79.

Hower, J. (1981a) X-ray diffraction identification of mixed-layer clay minerals: in *Clays and the Resource Geologists:* F. J. Longstaff, ed., Mineral. Assoc. Canada Short Course Handbook 7, 39–59.

Hower, J. (1981b) Shale diagenesis: in *Clays and the Resource Geologist*, F. J. Longstaff, ed., *Mineral. Assoc. Canada Short Course Handbook*, **7**, 60–80.

Hower, J., Eslinger, M. V., Hower, M., and Perry, E. A. (1976) Mechanism of burial metamorphism of argillaceous sediments: I—mineralogical and chemical evidences: *Geol. Soc. America Bull.* **87**, 725–737.

Hower, J. and Hall, M. L. (1970) Clay petrology of the upper Cretaceous Two Medicine Formation, central Montana: *Prog. Abstracts, 19th Annual Clay Minerals Conf., Miami, Florida*, p. 24.

Hower, J. and Mowatt, T. C. (1966) The mineralogy of illites and mixed-layer illite-montmorillonites: *Amer. Mineral.* **51**, 825–854.

Hunt, J. M. (1979) *Petroleum Geochemistry and Geology:* W. H. Freeman, San Francisco, 617 pp.

Iijima, A. and Utada, M. (1971) Present-day diagenesis of the Neogene geosynclinal deposits in the Niigata oilfield, Japan: in *Molecular Sieve Zeolites—I*, R. F. Gould, ed., Advances in Chemistry Series **101**, American Chemical Society, Washington, D.C., 342–349.

Iijima, A. and Utada, M. (1972) A critical review on the occurrence of zeolites in sedimentary rocks in Japan: *Japanese J. Geol. Geogr.* **42**, 81–83.

Iiyama, J. T. and Roy, R. (1963) Controlled synthesis of heteropolytypic (mixed-layer) clay minerals: in *Clays and Clay Minerals, Proc. 11th Natl. Conf., Ottawa, Ontario, 1958*, W. F. Bradley, ed., Pergamon Press, New York, 29–46.

Kohyama, N., Shimoda, S., and Sudo, T. (1973) Iron-rich saponite (ferrous and ferric forms): *Clays & Clay Minerals* **21**, 229–237.

Kopp, O. C. and Fallis, S. M. (1974) Corrensite in the Wellington Formation, Lyons, Kansas: *Amer. Mineral.* **59**, 623–624.

Kubler, B. (1963) Untersuchungen über die Tonfraction der Trias der Sahara: *Fortschr. Geol. Rheinl. Westf.* **10**, 319–324.

Kubler, B. (1973) La corrensite, indicateur possible de milleux de sédimentation et du degré de transformation d'un sediment: *Bull. Centre Rech. Pau-SNPA* **7**, 543–556.

Kubler, B., Martini, J., and Vuagnat, M. (1974) Very low grade metamorphism in western Alps: *Schweizer. Miner. Petrog. Mitt.* **54**, 461–469.

Lawrence, J. R., Drever, J. I., Anderson, T. F., and Brueckner, H. K. (1979) Importance of alteration of volcanic material in the sediments of Deep Sea Drilling site 323: chemistry, $^{18}O/^{16}O$ and $^{87}Sr/^{86}Sr$: *Geochim. Cosmochim. Acta* **43**, 573–588.

Lippmann, F. (1954) Über einen Keuperton von Zaisersweihe bei Maulbronn: *Heidelb. Beitr. Miner. Petrog.* **4**, 130–134.

Lippmann, F. (1956) Clay minerals from the Rot Member of the Triassic near Göttingen, Germany: *J. Sed. Petrol.* **26**, 125–139.

MacEwan, D. M. C. and Wilson, M. J. (1980) Interlayer and intercalation complexes of clay minerals: in *Crystal Structures of Clay Minerals and Their X-Ray Identification*, G. W. Brindley and G. Brown, eds., Mineralogical Society, London, 197–248.

Martin-Vivaldi, J. L. and MacEwan, D. M. C. (1957) Triassic chlorites from the Jura and the Catalan Coastal Range: in *Clays and Clay Minerals, Proc. 3rd Natl. Conf., Houston, Texas, 1956*, W. O. Milligan, ed., Natl. Acad. Sci., Natl. Res. Counc. Publ. **395**, Washington, D.C., 177–183.

Maurel, P. (1962) Etude minéralogique et géochimique des formations argileuses des environs de Saint-Affrique (Aveyron): *Bull. Soc. Franc. Mineral. Cristallogr.* **85**, 329–374.

McCubbin, D. G. and Patton, J. W. (1981) Burial diagenesis of illite-smectite, a kinetic model: *Amer. Assoc. Petrol. Geol. Bull.* **65**, 956.

Melson, W. G. and Thompson, G. (1973) Glassy abyssal basalts, Atlantic sea floor near St. Paul's rocks: petrography and composition of secondary clay minerals: *Geol. Soc. America Bull.* **84**, 703–716.

Perry, E. and Hower, J. (1970) Burial diagenesis in Gulf Coast pelitic sediments: *Clays & Clay Minerals* **18**, 165–177.

Peterson, M. N. A. (1961) Expandable chloritic clay minerals from Upper Mississippian carbonate rocks of the Cumberland Plateau in Tennessee: *Amer. Mineral.* **46**, 1245–1269.

Pevear, D. R. and Whitney, C. G. (1982) Clay minerals in Coast Range basalts of the Pacific Northwest: Eocene seafloor metamorphism?: in *Prog. Abstracts, 19th Ann. Meeting, Clay Minerals Society, Hilo, Hawaii, August, 1982*, p. 6.

Ponte, F. C., Fonseca, J. R., and Carozzi, A. V. (1980) Petroleum habitats in the Mesozoic-Cenozoic of the continental margin of Brazil: in *Facts and Principles of World*

Petroleum Occurrence, A. D. Miall, ed., Can. Soc. Pet. Geol., Memoir **6,** 857–885.

Reynolds, R. C. (1980) Interstratified clay minerals: in *Crystal Structures of Clay Minerals and Their X-ray Identification,* G. W. Brindley and G. Brown, eds., Mineralogical Society, London, 249–303.

Reynolds, R. C., Jr. and Hower, J. (1970) The nature of interlayering in mixed-layer illite-montmorillonite: *Clays & Clay Minerals* **18,** 25–36.

Scarfe, C. M. and Smith, D. G. W. (1977) Secondary minerals in some basaltic rocks from DSDP leg 37: *Canadian J. Earth Sci.* **14,** 903–910.

Schoonmaker, J. (1986) Clay mineralogy and diagenesis of sediments from deformation zones in the Barbados accretionary prism (DSDP leg 78A): in *Synthesis of Structural Fabrics of Deep Sea Drilling Project Cores from Forearcs,* J. D. Moore, ed., Geol. Soc. Amer., Boulder, Colorado, Memoir **166** (in press).

Seyfried, W. E., Jr. and Bischoff, J. L. (1979) Low-temperature basalt alteration by seawater: an experimental study at 70° and 150°C: *Geochim. Cosmochim. Acta* **43,** 1937–1947.

Seyfried, W. E., Jr., Shanks, W. C., 3rd, and White, D. E. (1978) Clay mineral formation in DSDP leg 37 basalt: *Earth Planet. Sci. Letters* **41,** 265–276.

Sigvaldason, G. and White, D. E. (1961) Hydrothermal alteration of rocks in two drill holes at Steamboat Springs, Washoe County, Nevada: *U.S. Geol. Surv. Prof. Pap.* **424D,** 116–122.

Stephen, I. and MacEwan, D. M. C. (1951) Chlorite minerals of an unusual type: *Clay Mineral. Bull.* **1,** 157–162.

Sudo, T. (1954) Iron-rich saponite found from Tertiary iron sand beds in Japan: *J. Geol. Soc. Japan* **59,** 18–27.

Sudo, T. and Shimoda, S. (1978) *Clays and Clay Minerals of Japan:* Elsevier, Amsterdam, 326 pp.

Suzsczynski, E. (1970) La géologie et la tectonique de la Plataform Amazonienne: *Geol. Rundschau* **59,** 1232–1253.

Tardy, Y. and Garrels, R. (1974) A method of estimating the Gibbs energies of formation of layer silicates: *Geochim. Cosmochim. Acta* **38,** 1101–1116.

Tomasson, J. and Kristmannsdottir, H. (1972) High temperature alteration minerals and thermal brines, Reykjanes, Iceland: *Contr. Mineral. Petrol.* **36,** 123–134.

Velde, B. (1977) A proposed phase diagram for illite, expanding chlorite, corrensite and illite-montmorillonite mixed-layered minerals: *Clays & Clay Minerals* **25,** 264–270.

Weaver, C. E. (1979) Geothermal alteration of clay minerals and shales: diagenesis: *ONWI Technical Report* **21,** 176 pp.

Whitney, G. (1983) Hydrothermal reactivity of saponite: *Clays & Clay Minerals* **31,** 1–7.

Wilson, M. J. (1971) Clay mineralogy of the Old Red Sandstone (Devonian) of Scotland: *J. Sed. Petrol.* **41,** 995–1007.

Wilson, M. J., Bain, D. C., and Mitchell, W. A. (1968) Saponite from the Dalradian meta-limestones of North-East Scotland: *Clays & Clay Minerals* **7,** 343–349.

Wyart, J. and Sabatier, G. (1966) Synthèse hydrothermale de la corrensite: *Bull. Groupe Fr. Argiles* **18,** 33–40.